

pubs.acs.org/cm Article

# Acid-Assisted Soft Chemical Route for Preparing High-Quality Superconducting 2M-WS<sub>2</sub>

Xiaoyu Song, <sup>L</sup> Brianna Hoff, <sup>L</sup> Ratnadwip Singha, Joseph W. Stiles, Grigorii Skorupskii, Jason F. Khoury, Guangming Cheng, Franziska Kamm, Ayelet J. Uzan, Stephanie Dulovic, Sanfeng Wu, Florian Pielnhofer, Nan Yao, and Leslie M. Schoop\*



Cite This: Chem. Mater. 2023, 35, 5487-5496



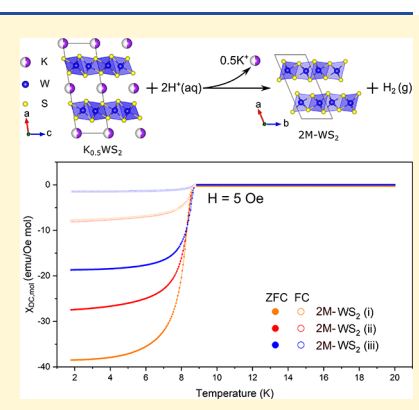
**ACCESS** I

Metrics & More

Article Recommendations

Supporting Information

ABSTRACT: 2M-WS<sub>2</sub> is a metastable, superconducting polymorph of the transition metal dichalcogenide (TMD) WS<sub>2</sub>, comprised of layers of face-sharing distorted WS<sub>6</sub> octahedra. It is predicted to host non-Abelian quantum states, promising for topological computing. Due to its thermodynamic instability, 2M-WS<sub>2</sub> cannot be synthesized using solid-state synthesis. Rather, it requires a top-down approach in which  $K^+$  is deintercalated from  $K_xWS_2$ ; so far, this process has been completed using a strong oxidizer,  $K_2Cr_2O_7$  in dilute  $H_2SO_4$ . A disadvantage of such an indirect synthesis is that the harsh reaction condition may cause the crystal quality to suffer. To date, no studies have been performed to optimize the synthesis or understand the chemical nature of this reaction. In this study, we found that the K-deintercalation process from  $K_xWS_2$  is spontaneous, and a non-oxidative acidic reaction environment is sufficient to facilitate the oxidation of  $K_xWS_2$  to  $2M-WS_2$  while reducing  $H^+$  to  $H_2$ . By analyzing the superconducting transition in the heat capacity, we found that  $2M-WS_2$  made using less aggressive methods has higher superconducting volume fractions. We describe how to access the thermodynamically unfavorable superconducting 2M phase of  $WS_2$  as high-quality crystals.



## ■ INTRODUCTION

Transition metal dichalcogenides (TMDs) with a chemical formula of  $MX_2$  (M = transition metal, X = chalcogenide) are a class of van der Waals (vdW)-layered materials with multiple structural polymorphs, which have diverse properties that are attractive for both fundamental research and potential applications. For example, WS<sub>2</sub> has two polymorphs, the semiconducting 2H-WS<sub>2</sub> and the superconducting 2M-WS<sub>2</sub>, where the number "2" refers to the number of layers in the unit cell, and the capital letters "H" and "M" refer to the polymorphs' hexagonal and monoclinic space groups, respectively. WS<sub>2</sub> naturally grows in the 2H phase, where each 1H layer is composed of face-sharing trigonal prismatic WS<sub>6</sub>. It has been widely studied for applications in optoelectronics, 1-6 valleytronics, 7-9 and as a catalyst for hydrogen evolution. 10-12 The 2M phase consists of 1T'-WS<sub>2</sub> layers of face-sharing distorted WS<sub>6</sub> octahedra, <sup>13</sup> where the "T" refers to the octahedral coordination of the metal atoms and the "'" refers to the distorted octahedral structure. 14 The monolayer is predicted to be a topological insulator.<sup>15</sup> The bulk 2M phase is superconducting below 8.8 K<sup>16</sup> and has the potential to host quantum states obeying non-abelian statistics, making it a promising building block for topological quantum computing. 17-20 Other TMDs with the same monolayer structure (the stacking can vary) are also known superconductors. Examples include gated WTe2 monolayers,

bulk WTe<sub>2</sub> under pressure,  $^{23,24}$  strained thin flakes of WTe<sub>2</sub>,  $^{25}$  bulk MoTe<sub>2</sub> in its 1T′ phase,  $^{26}$  and 1T′-MoS<sub>2</sub> monolayers.  $^{27,28}$  Out of these, 2M-WS<sub>2</sub> has the highest superconducting transition temperature. 2M-WS<sub>2</sub> has been chemically exfoliated to monolayers, and thin films composed of many overlapping monolayers were shown to superconduct below 7.3 K.  $^{29}$ 

 $2M\text{-WS}_2$  was first synthesized by oxidatively deintercalating potassium from  $K_xWS_2$  with  $K_2Cr_2O_7$  in dilute  $H_2SO_4$ . Recently, Lai et al. reported that  $I_2$  in acetonitrile can also fully deintercalate potassium from the starting compound to yield  $2M\text{-WS}_2$ . Although soft-chemical synthesis methods are powerful in accessing such thermodynamically metastable phases, they may lead to unexpected features, such as protonated products or defects and impurities. Furthermore, Heising and Kanatzidis reported that a protonated  $H_xWS_2$ , which is structurally similar to  $2M\text{-WS}_2$ , can be made by soaking  $LiWS_2$  in concentrated HCl. Conversely,  $2M\text{-WS}_2$  made with dilute  $K_2Cr_2O_7$  in  $H_2SO_4$  and well studied in the condensed matter physics community is thought to be

Received: April 6, 2023 Revised: June 25, 2023 Published: July 13, 2023





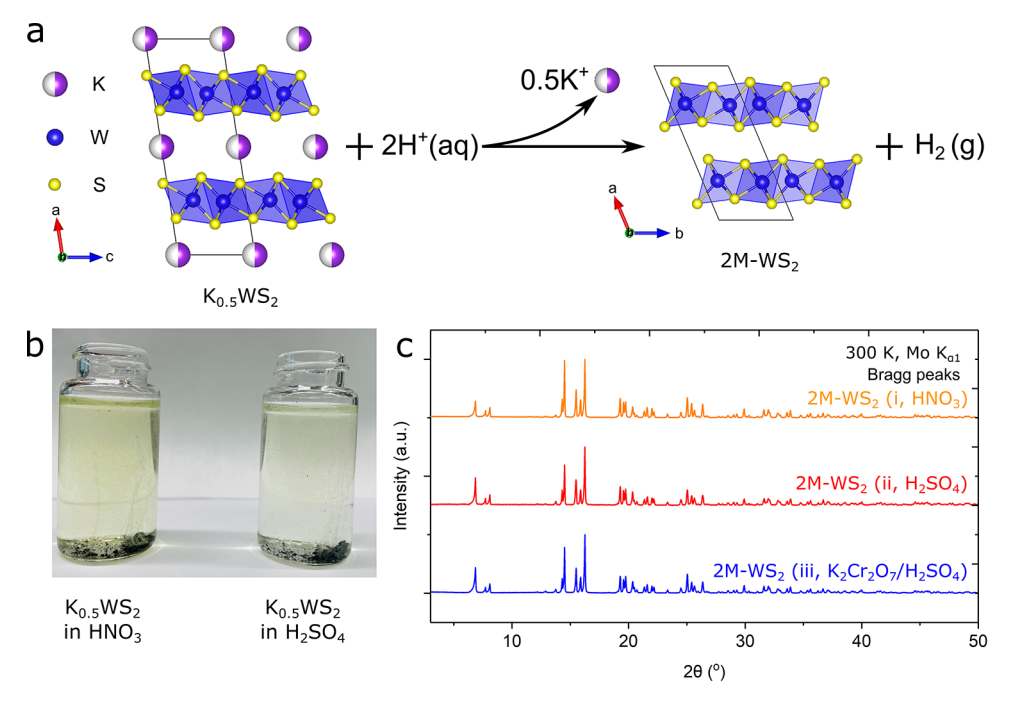


Figure 1. (a) Illustration of the oxidative K-deintercalation process of  $K_{0.5}WS_2$ . (b) Picture showing the  $H_2$  bubbles produced by reacting  $K_{0.5}WS_2$  with dilute  $H_2SO_4$  and  $HNO_3$ , respectively. (c) Powder X-ray diffraction (PXRD) of 2M-WS<sub>2</sub> synthesized by three different routes.

unprotonated, though with little evidence substantiating this claim. Additionally, prior studies on bulk 2M-WS<sub>2</sub> have not reported on crystal quality. Thus, it is unclear how much defects—such as residual K<sup>+</sup> between the layers, commonly found in deintercalated samples,  $^{32}$  or S vacancies that may result from over-oxidation—affect the properties. For example, the resistivity of a mechanically exfoliated  $1T^\prime$ -WS<sub>2</sub> monolayer does not drop to zero.  $^{30}$  It may be that the aggressive synthesis involving strongly oxidizing reagents, such as  $K_2Cr_2O_7$ , introduces defects to the samples, which would disrupt the electronic structure and superconductivity. Therefore, improving the synthesis and using gentler alternative methods are of great interest to providing high-quality single crystals or monolayers of this promising superconductor for future studies of its physical properties.

In this study, we report a new method to synthesize superconducting 2M-WS<sub>2</sub> starting from K<sub>0.5</sub>WS<sub>2</sub>, using dilute acid. We tested dilute H2SO4 and HNO3 and found that both are sufficient to oxidize  $K_{0.5}WS_2$  to  $2M\text{-}WS_2$  while reducing protons to H<sub>2</sub> gas bubbles. Thus, using aggressive oxidizing agents, such as K<sub>2</sub>Cr<sub>2</sub>O<sub>7</sub>, is unnecessary. We compare the structure and superconducting properties of the 2M-WS<sub>2</sub> synthesized with different reaction conditions: condition (i) dispersing K<sub>x</sub>WS<sub>2</sub> in dilute HNO<sub>3</sub>, condition (ii) using dilute H<sub>2</sub>SO<sub>4</sub>, and condition (iii) repeating the reported method using K<sub>2</sub>Cr<sub>2</sub>O<sub>7</sub> in dilute H<sub>2</sub>SO<sub>4</sub>. We found that 2M-WS<sub>2</sub> synthesized with any of the three conditions does not show evidence of S-H bonds or interstitial water, confirming that the superconducting phase is indeed proton-free. The samples synthesized with dilute HNO<sub>3</sub> and dilute H<sub>2</sub>SO<sub>4</sub> (conditions (i) and (ii)) show a higher superconducting fraction, establishing that samples of higher quality can be obtained with more gentle methods.

Finally, we found with Raman spectroscopy that laser irradiation with high laser intensity, regardless of laser wavelength, can induce a phase transformation from the 2M phase to the semiconducting 2H phase; thermal annealing

above  $\sim$ 220 °C has the same effect. While this observation rules out annealing as a way to cure defects and further improve crystal quality, it provides opportunities to create interfaces of super- and semiconducting WS<sub>2</sub>.

## EXPERIMENTAL DETAILS

**Materials and Synthesis.** Synthesis of  $K_{0.5}WS_2$   $K_{0.5}WS_2$  was synthesized by high-temperature solid-state methods reported previously; its crystal structure and chemical composition were reported in the same paper. Synthesis of 2M-WS<sub>2</sub> in Dilute Acids To fully remove the potassium, the  $K_xWS_2$  crystals were shaken in 0.02 M HNO<sub>3</sub> (i) or 0.01 M  $H_2SO_4$  (ii) with a solid-to-liquid ratio of 1 mg to 1 mL for 48 h. The crystals were cleaned with MilliQ water and dried at room temperature before further characterization. Synthesis of 2M-WS<sub>2</sub> with  $K_2Cr_2O_7$  in Dilute  $H_2SO_4$  This synthesis was repeated, as reported earlier.

Plastic spatulas, plastic tweezers, and ceramic blades were used throughout the experiments. No stainless steel-based tools were used in the synthesis to avoid potential contamination.

Characterization. Powder X-ray diffraction (PXRD) data were collected on a STOE STADI P PXRD with Mo  $K_{\alpha 1}$  radiation and a single-Mythen detector, working in Debye–Scherrer geometry. Crystals were ground with ground amorphous quartz capillary powders in a 1:1 volume ratio before being sealed in 0.5 mm amorphous quartz capillaries for the measurements.

**Gas Chromatography (GC)** was used to measure the generated gas with an SRI 8610C gas chromatography with ultra high purity Ar flow. It used a 30MXT502 column and thermal conductivity detector. For detecting  $\rm H_2$ , 50 microliters of the headspace was injected for a 10 min isotherm at 80 °C.

Scanning electron microscopy (SEM) images and energy-dispersive spectroscopy (EDS) spectra were taken with a Verios 460 extreme high-resolution scanning electron microscope with an Oxford energy dispersive X-ray spectrometer and with a Quanta 200 FEG environmental-SEM. X-ray photoelectron spectroscopy (XPS) data were collected on a ThermoFisher K-Alpha X-ray photoelectron spectrometer. The sample was either freshly cleaved with scotch tape or etched with low energy Ar ions to reduce the influence of possible surface contamination and oxidation. The data were analyzed using CasaXPS and referenced to the C 1s transition of adventitious carbon

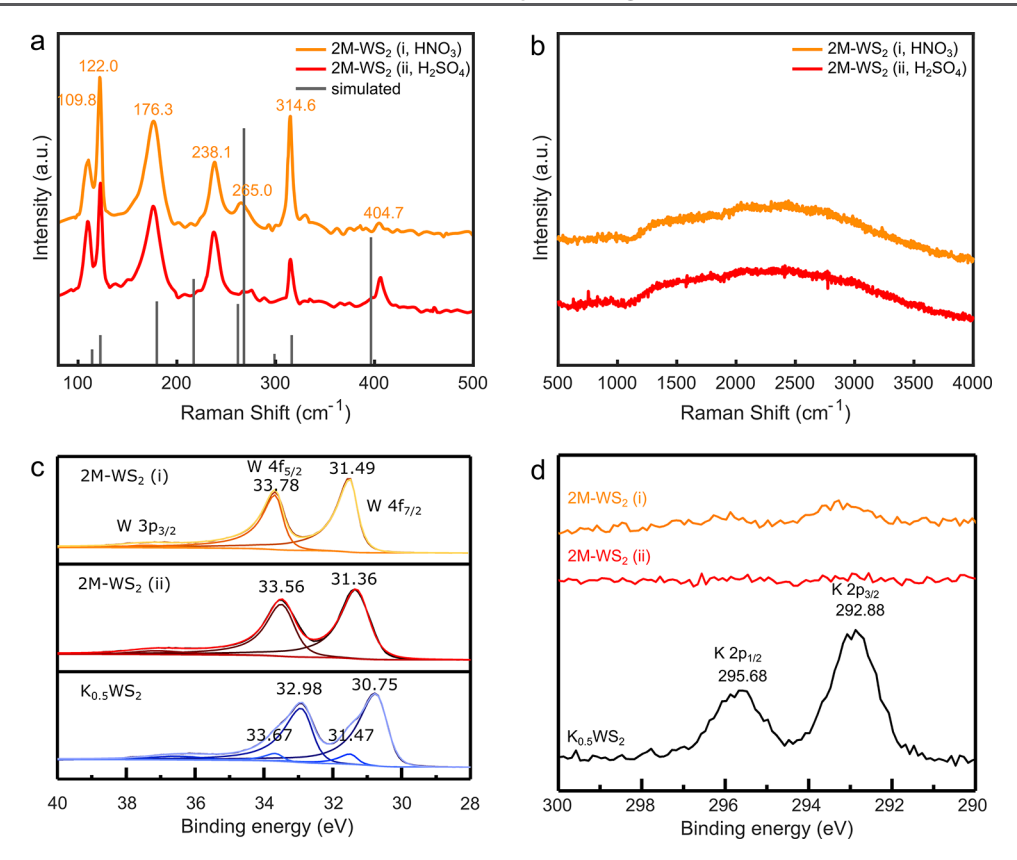


Figure 2. (a,b) Raman spectra at low Raman shift region (a) and high Raman shift region (b) of 2M-WS<sub>2</sub> crystals made with methods (i) and (ii), compared with the simulated Raman vibration based on the unprotonated 2M-WS<sub>2</sub>'s structure. (c,d) W (c) and K (d) XPS spectra of 2M-WS<sub>2</sub> crystals made with methods (i) and (ii) in comparison with the spectra of pristine  $K_{0.5}WS_2$ .

which was calibrated to 284.5 eV binding energy. Thermogravimetric analysis (TGA) was performed under airflow with a PerkinElmer TGA-8000 thermogravimetric analyzer. Raman spectra were obtained using a Horiba Raman spectrometer with a 633 and 532 nm laser source; the laser power was 19.0 and 9.13 mW when measured under a 100× objective, respectively. When using the 633 nm laser, a neutral-density (ND) filter of 0.3 or larger was used to prevent the laser-induced phase transformation and no ND filter was used to induce the phase transformation on the crystals. When using the 532 nm laser, an ND filter of 0.6 or larger was used to prevent the laser-induced phase transformation and an ND filter of 0.3 was used to induce the phase transformation on the crystals. Differential scanning calorimetry (DSC) was performed using a PerkinElmer differential scanning calorimeter with HyperDSC DSC8500 at a heating rate of 10 °C min<sup>-1</sup> and a cooling rate of 20 °C min<sup>-1</sup>.

High-resolution cross-sectional scanning transmission electron microscopy (STEM) images were taken with a Titan Cubed Themis 300 double Cs-corrected S/TEM. The samples were cut and transferred onto a Cu TEM grid with a Helios NanoLab G3 UC DualBeam FIB/SEM. Details of cross-sectional TEM sample preparation were previously described here 31,32

Superconductivity Measurements. The heat capacity and magnetic measurements were performed on a physical properties measurement system (PPMS, Quantum Design) and magnetic property measurement system (MPMS, Quantum Design), respectively. The direct current (d.c.) measurements were performed with a 5 Oe external applied magnetic field. All superconductivity measurements were done on powder samples.

#### RESULTS AND DISCUSSION

**Exploration of the Synthesis Conditions with Dilute Acids.** To improve the quality of 2M-WS<sub>2</sub> crystals, we aimed to find a less aggressive oxidizing reagent. We chose to

investigate two new reaction conditions: (i) dilute HNO<sub>3</sub> and (ii) dilute H<sub>2</sub>SO<sub>4</sub> (without K<sub>2</sub>Cr<sub>2</sub>O<sub>7</sub>) and compare the products to the reported method (iii) using K<sub>2</sub>Cr<sub>2</sub>O<sub>7</sub> in dilute H<sub>2</sub>SO<sub>4</sub>. As soon as the crystals come into contact with the dilute acids (Figure 1a), generated gas bubbles can be observed, as shown in Figure 1b. GC analysis of the generated gas bubbles from conditions (i) and (ii) identifies these as H<sub>2</sub> gas (Figure S1). Thus, protons are reduced to H2, while  $K_{0.5}WS_2$  is oxidized. Importantly, we found no  $H_2S$  or  $SO_x$ present in the headspace, indicating that the gas formation was not a product of over-oxidation or decomposition of the materials. PXRDs of the reaction products made using the three conditions are shown in Figure 1c. The peak positions of all three compounds match the simulated ones for 2M-WS<sub>2</sub> (Figure S6), suggesting that suspending  $K_{0.5}WS_2$  in either dilute nitric acid or sulfuric acid also successfully yields 2M-WS<sub>2</sub>. We found that the reaction completes faster with condition (iii) due to the aid of the additional oxidizing agent. As we discuss in the supporting information (SI, Sections 2) and 3), the reactions using only acids require more time to fully remove K<sup>+</sup>, and interstitial water molecules appear only if some K<sup>+</sup> remains between the layers.

**Redox Reaction or Proton-Exchange Reaction?** Thus far, we have assumed that the reaction of  $K_{0.5}WS_2$  in acid is entirely oxidative. Alternatively, it could be interpreted as solely a proton exchange between  $K^+$  with  $H^+$  or a combination of partial oxidation and partial proton exchanges. We used Raman spectroscopy to rule out the presence of protons in the samples and confirm that the end product is indeed  $2M-WS_2$ . To do this, we investigated whether a S-H bond is forming since S-H bonds have characteristic stretches. Both  $2M-WS_2$ .

samples made with different dilute acids show typical Raman vibrations in the low Raman shift region, as reported in the earlier studies, and fit well with the DFT simulations based on the structural model of unprotonated 2M-WS<sub>2</sub> (Figure 2a). No intense additional vibration modes appear, neither in the low nor high Raman shift region, which would indicate S-H bond stretches (Figure 2b). 31,35 DFT calculations show that these vibrations would occur between 450 and 660 cm<sup>-1</sup> and above 2000 cm<sup>-1</sup> (S-H stretching vibration). The protonated models and corresponding calculated Raman spectra are shown in Figures S7 and S8. We then used XPS to determine that W was oxidized upon treatment with dilute acid. We performed XPS analysis on both pristine K<sub>0.5</sub>WS<sub>2</sub> and 2M-WS<sub>2</sub> crystals. As shown in Figure 2c, the parent compound K<sub>0.5</sub>WS<sub>2</sub> (dark blue) has a binding energy of 30.75 and 32.98 eV for the W  $4f_{7/2}$  and  $4f_{5/2}$  peaks, respectively. The W  $4f_{7/2}$  and  $4f_{5/2}$ peaks of 2M-WS<sub>2</sub> appear at binding energies of 31.49 and 33.78 eV, respectively (condition 1) and 31.36 and 33.56 eV, respectively (condition 2). As the S ligand environment does not change, this suggests that W is in a lower oxidation state in  $K_{0.5}WS_2$  and that the reaction is indeed oxidative. Furthermore, the absence of K 2p peaks in the XPS spectrum confirms the removal of K in 2M-WS<sub>2</sub> synthesized via conditions (i) and (ii) in comparison with the  $2p_{1/2}$  and  $2p_{3/2}$  peaks observed in the parent compound K<sub>0.5</sub>WS<sub>2</sub>. However, small peaks in the crystal prepared by condition (i) indicate there may be trace amounts of K present.

In addition, the XPS spectrum of  $K_{0.5}WS_2$  exhibits a shoulder in the  $4f_{5/2}$  peak and the  $4f_{7/2}$  peak, at 33.67 and 31.47 eV, respectively (Figure 2c, blue). The origin of these shoulders is due to the half-occupied state of  $K^+$ . As a result, some of the W is influenced by  $K^+$  interactions, whereas some of the W behaves as though no  $K^+$  were present.

The increase of binding energy of the W 4f peaks from  $K_{0.5}WS_2$  to  $2M\text{-}WS_2$ , as well as the absence of a S–H vibration together and the observation of  $H_2$  bubbles produced during the reaction clearly show that the reaction is a redox reaction instead of proton-exchange reaction and dilute acids are sufficient to oxidize W from  $3.5^+$  in  $K_{0.5}WS_2$  to  $4^+$  in  $WS_2$ . The proposed reaction formula is as follows:

$$4K_{0.5}WS_2(s) + 2H^+(aq)$$
  
 $\rightarrow 4 2M-WS_2(s) + 2K^+(aq) + H_2(g)$ 

Here we refer to the standard reduction potentials, as shown in Table 1, to discuss the choice of oxidizing reagents for  $K_xWS_2$  from the two reported methods ( $I_2$  in acetonitrile and  $K_2Cr_2O_7$  in dilute  $H_2SO_4$ ) in comparison to the method used in this study (dilute acids). Based on our experimental results, an acidic environment (2  $H^+$  (aq) + 2  $e^- \rightleftharpoons H_2$  (g)) is enough

Table 1. Table of Standard Reduction Potentials for the Selected Half-Reactions

half-reactions	$E^{\circ} (V)^{36,37}$
$2 \text{ H}^+ \text{ (aq)} + 2 \text{ e}^- \rightleftarrows \text{ H}_2 \text{ (g)}$	0.00
$I_3^- + 2 e^- \rightleftarrows 3 I^{-a}$	$0.32^{b}$
$Cr_2O_7^{2-}$ (aq)+ 14 H <sup>+</sup> (aq) + 6 e <sup>-</sup> $\rightleftharpoons$ 2 $Cr^{3+}$ (aq) + 7 H <sub>2</sub> O (l)	1.36 <sup>c</sup>

 $^a\mathrm{The}$  redox potential was determined in acetonitrile.  $^b\mathrm{This}$  value was calculated from voltammetry experiments taken at 24 °C and 1 atm.  $^c\mathrm{This}$  value was calculated from voltammetry experiments taken at 25 °C and 1 atm.

to fully remove  $K^+$ .  $I_2$  in acetonitrile, with a chemical potential of 0.32 V, can also enable this reaction and, indeed, has been reported as a way to make 2M-WS<sub>2</sub> from  $K_x$ WS<sub>2</sub>.<sup>30</sup> It is clear then that  $Cr_2O_7^{2-}$ , with a chemical potential of 1.36 V, is unnecessary for completely removing  $K^+$ . However, it is also understandable why the reaction completes much faster—one hour versus 48 hours—than that of the acid.

Characterization of 2M-WS<sub>2</sub> Made by Three Different Routes. To determine how the different reaction conditions affect the resulting crystal structure, we studied the PXRD and HRSTEM to look for any discrepancies between the 2M-WS<sub>2</sub> formed by the three conditions. As shown in Figure S6, Rietveld refinements were conducted on all three obtained PXRD patterns. The lattice parameters for all three samples match within 0.1 Å of the reported literature values and 0.01 Å of each other. Thus, the PXRD patterns show no evident structural differences between any of the three samples. Furthermore, there were no differences between full width at half maximum values for the three PXRD patterns, suggesting similar crystallite domain sizes. Similarly, HRSTEM images did not give any indication of structural differences between the samples. The diffraction pattern (DP) of the studied areas (Figure 3a-c) fit well with the simulation for the [010] plane,

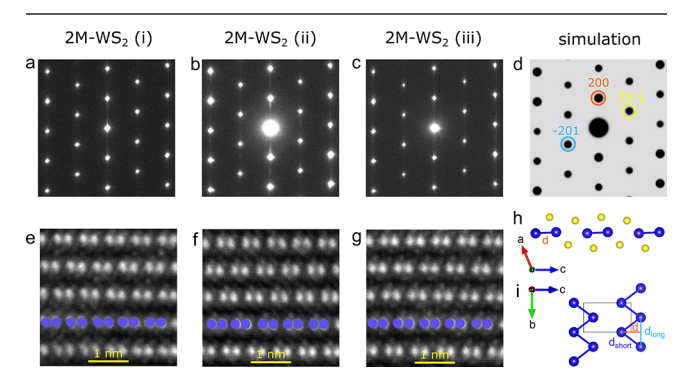


**Figure 3.** (a–c) Selected area electron diffraction pattern of the cross-sectional 2M-WS $_2$  samples prepared by conditions i (a), ii (b), and iii (c). (d) Simulated electron diffraction pattern of 2M-WS $_2$ , zone axis <0 1 0>. (e–g) High-resolution scanning transmission electron microscopy images of the [0 1 0] planes of 2M-WS $_2$  samples prepared by methods i (e), ii (f), and iii (g). (h) Structure of the [0 1 0] planes of 2M-WS $_2$  showing the W–W pairs. Blue and yellow spheres represent for W and S atoms, respectively. (i) W chains in the [1 0 0] planes.

Figure 3d, using the refined structure parameters obtained from PXRD (Figure S6). The d-spacings of three DPs shown in Figure 3a-c are the same, corroborating the conclusion that the lattice parameters are nearly identical, as found by PXRD. A typical cross-sectional HRSTEM image for 2M-WS<sub>2</sub> synthesized with each method is shown in Figure 3e-g. VdW layers of 1T'-WS2, where the W atoms (blue) sit in a distorted octahedron of S atoms (yellow) (Figure 3h), are clearly visible in Figure 3e-g, suggesting high crystallinity and homogeneity of the 2M-WS2 phase. The 2M-WS2 crystals maintain the vdW layered structure with no observable atoms occupying the interlayer space in the conditions used in this study. No difference in defect concentration between the three samples could be detected. However, as the S atoms appear very faint compared to the W atoms in HRSTEM, differences in S defects might be unobserved. In general, the structural analysis indicates no difference between the samples. Still,

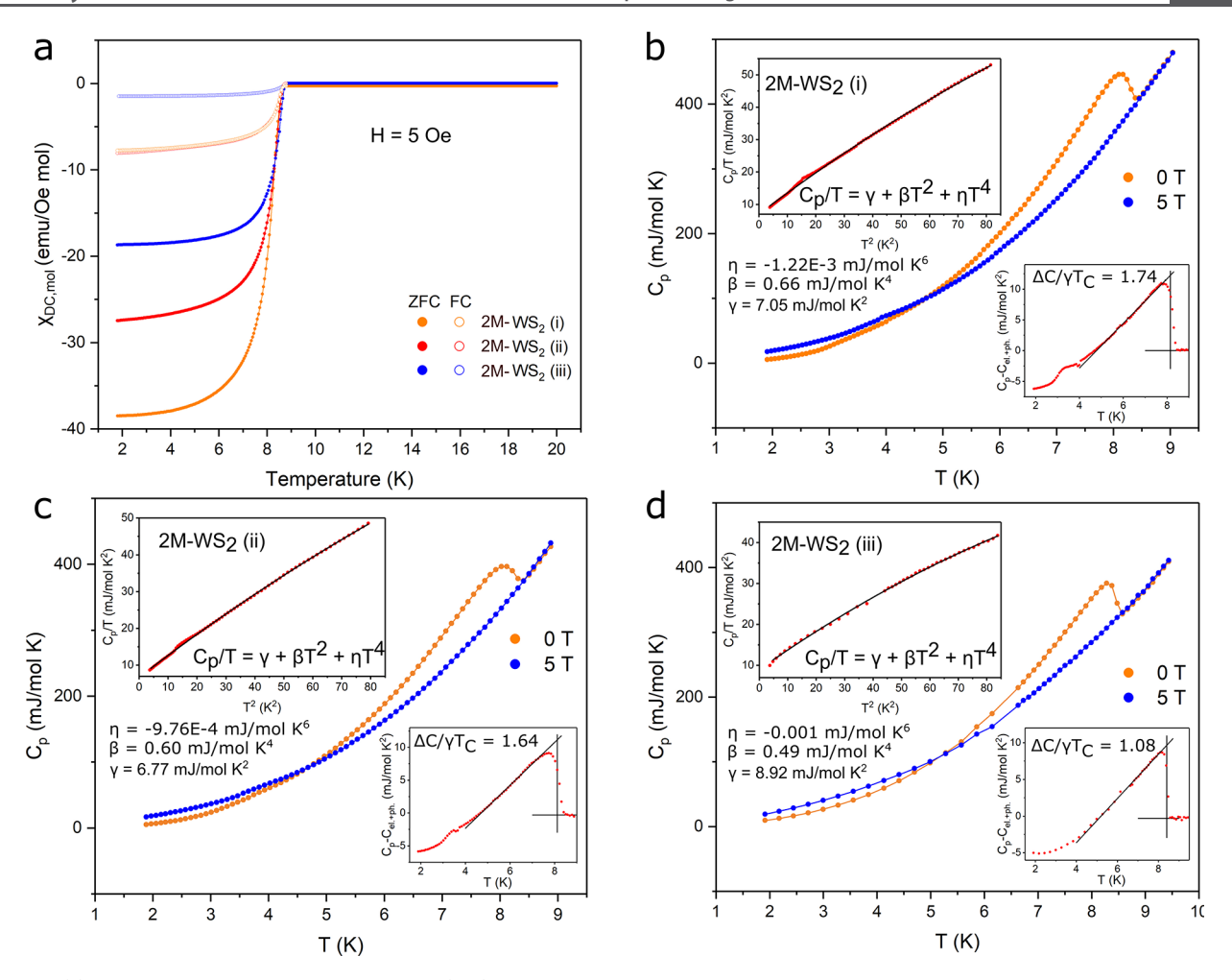


Figure 4. (a) Temperature dependent direct current (d.c.) magnetic susceptibility of 2M-WS<sub>2</sub> synthesized with the three reaction conditions. (b) Heat-capacity ( $C_p$ -T) of 2M-WS<sub>2</sub> synthesized with dilute HNO<sub>3</sub> (condition (i)), (c) dilute H<sub>2</sub>SO<sub>4</sub> (condition (ii)), and (d) K<sub>2</sub>Cr<sub>2</sub>O<sub>7</sub> in dilute H<sub>2</sub>SO<sub>4</sub> (condition (iii)). Upper left insets show  $C_p$ /T vs T<sup>2</sup> (red) and its fitting (black) when the superconductivity is suppressed by a field of 5 T. The bottom right insets show ( $C_p$ -C<sub>el.+ph.</sub>) vs T from 2 to 10 K in the superconducting state. The black lines are guides for estimating T<sub>c</sub> and the superconducting jump  $\Delta$   $C/\gamma T_c$ .

PXRD could miss amorphous side phases, and the HRSTEM of a selected FIB-cut crystal is only a fraction of one piece of crystal, and thus, also does not provide a complete picture. A more sensitive way to analyze sample quality is to probe the physical properties, in this case, the superconductivity.

Comparison of Superconducting Properties of 2M-WS<sub>2</sub> Synthesized with Different Methods. To determine whether the new synthetic method yields crystals of higher quality due to the omission of a harsh oxidant, we studied and compared the superconducting performance of the crystals prepared via the three reaction conditions. Figure 4a shows the temperature-dependent d.c. magnetic susceptibility for the 2M-WS<sub>2</sub> crystals in zero-field cooling (ZFC) and field cooling (FC) conditions under an applied magnetic field of 5 Oe. The superconducting transition appears at 8.8 K for all three 2M-WS2 crystals made with different conditions, which agrees with the reported transition temperature for 2M-WS<sub>2</sub>. 16,30 As expected, due to the Meissner-Ochsenfeld effect, the diamagnetic response is much smaller for FC scans. The d.c. measurements reveal that the separate samples differ in quality; the minimum  $\chi_{mol}$  of 2M-WS<sub>2</sub> made by each condition increases in negativity in the order (iii), (ii), and (i), suggesting that the sample prepared with condition (i) has the strongest repulsion of the magnetic field, followed by that of (ii). It also

suggests that condition (i)-crystals have the largest superconducting volume fraction and that other methods may introduce non-superconducting impurities. This experiment was repeated with the second batch (shown in the SI, Figure S9), and again, the samples made with the new method expelled the magnetic field most efficiently. All of our results show that HNO<sub>3</sub> consistently gives better samples as compared to H<sub>2</sub>SO<sub>4</sub>. The concentration for each acid was chosen so that the proton concentration is the same, thus, suggesting HNO<sub>3</sub> is a better acid for this synthesis. Further studies testing other acids and concentrations might push the superconducting volume fraction of 2M-WS<sub>2</sub> samples even higher.

The heat-capacity (HC) measurements of the three differently synthesized 2M-WS<sub>2</sub> are shown in Figure 4b–d. A peak is observed around the superconducting temperature in all three samples, indicating bulk superconductivity (i.e., the majority of each sample is in the superconducting phase). The normal state behavior of each sample between 2 and 10 K under an applied magnetic field of 5T, where the superconductivity is suppressed, can be fitted with  $C_p/T = \gamma + \beta T^2 + \eta T^4$ , where  $\gamma$  is the Sommerfeld coefficient, corresponding to the electronic contribution to  $C_p$ , and the two terms  $\beta T^2$  and  $\eta T^4$  are related to the phononic contribution. <sup>38,39</sup> The fitted values of  $\gamma$ ,  $\beta$ , and  $\eta$  of each material are shown in Figure 4b–d.

Using the equal area construction, we estimate the specific heat jump  $\Delta$   $C/\gamma$   $T_c$  for three crystals to be 1.74 (condition (i)), 1.64 (condition (ii)), and 1.08 (condition (iii)), respectively. Notably, the values found for the conditions using the newly developed method here are closer to the expected value of 1.43 for BCS superconductivity. Thus, the specific heat also shows that the sample quality of samples made with conditions (i) and (ii) is significantly higher than those made with condition (iii). The higher values for  $\Delta$   $C/\gamma$   $T_c$  observed in conditions (i) and (ii) are correlated with their lower Sommerfeld parameters  $\gamma$  (see Table 2). Since the Sommerfeld parameter is a measure

Table 2. Superconducting Properties of 2M-WS<sub>2</sub> Synthesized via Different Routes

parameters	units	2M-WS <sub>2</sub>	2M-WS <sub>2</sub>	2M-WS <sub>2</sub>
		$(HNO_3)$	$(H_2SO_4)$	$(K_2Cr_2O_7 \text{ in } H_2SO_4)$
$T_{\rm c}$ (d.c.)	K	8.8	8.8	8.8
$T_{\rm c}$ (HC)	K	8.3	8.2	8.4
γ	mJ/mol K <sup>2</sup>	7.05	6.77	8.92
$\Delta$ $C/\gamma$ $T_{\rm c}$	\	1.74	1.64	1.08
$\Theta_{ m D}$	K	206.7	213.4	228.4
$\lambda_{ m ep}$	\	0.90	0.88	0.88

of the density of states (DOS) at the Fermi level, the lower values might be correlated with lower defects, as defects would enhance the DOS. The Debye temperature  $(\Theta_D)$  and the

electron-phonon coupling constant ( $\lambda_{ep}$ ) for each compound are listed in Table 2.  $\lambda_{ep}$  is  $\sim$  0.9 for all samples, suggesting weak to intermediate electron-phonon coupling.<sup>40</sup>

Phase Transformation of 2M-WS<sub>2</sub> to 2H-WS<sub>2</sub>. As discussed, 2M-WS<sub>2</sub> is a metastable phase that cannot be synthesized directly from the elements. While bulk 2M-WS<sub>2</sub> crystals are not sensitive to air and can be stored under inert conditions, we found that they are susceptible to heat and laser irritation. It was reported that on a 2M-WS<sub>2</sub> nanosheet, a laser beam of 532 nm can induce a phase transformation from the 2M phase to the semiconducting 2H phase.<sup>41</sup> In this study, we found that this phenomenon is independent of the sample thickness or laser wavelength and, thus, further studied its mechanism.

As shown in Figure 5a,b, on an area where the Raman spectrum confirms the 2M structure when measured with a lower intensity laser, increasing the laser intensity while keeping the wavelength, induces a phase transition as evidenced by the appearance of the characteristic  $E_{\rm g}$  and  $A_{\rm 2g}$  peaks of the 2H phase. This phenomenon is repeatable on 2M-WS<sub>2</sub> crystals made with all three conditions. The phase transformation can be induced by both red (633 nm) and green (532 nm) lasers as long as the laser intensity exceeds a certain threshold, suggesting this laser-induced phase transformation process is likely caused by the heat generated by the laser

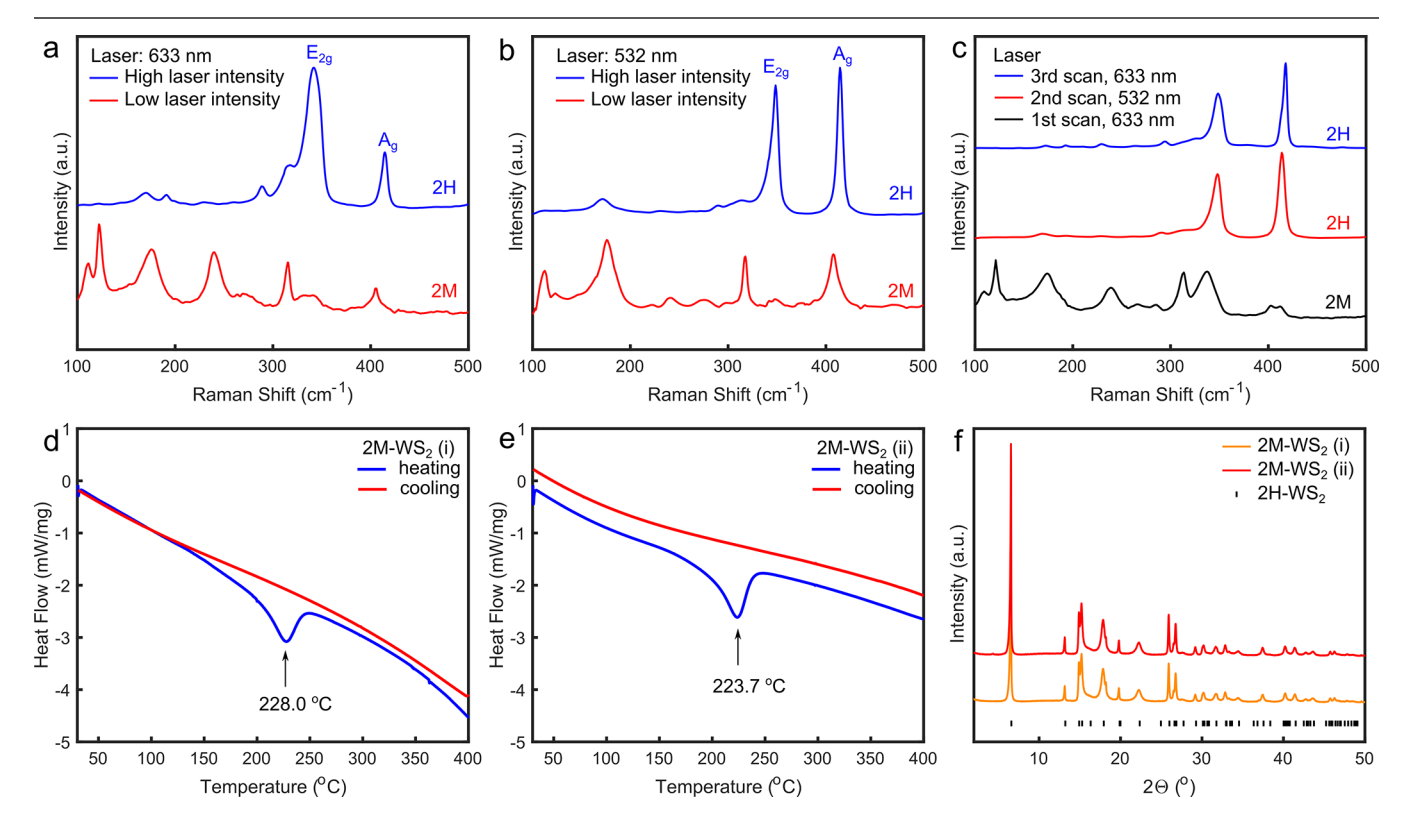


Figure 5. (a,b) Laser induced phase transformation from 2M-WS<sub>2</sub> to 2H-WS<sub>2</sub> with either 633 nm (a) or 532 nm (b), respectively. On the same spot of the crystal, starting from measuring with a low intensity laser, the Raman spectrum shows typical vibrations of 2M-WS<sub>2</sub> (red). After increasing the laser intensity, the Raman spectrum shows typical vibrations for 2H-WS<sub>2</sub> (blue). (c) Laser induced phase transformation measured on the same spot of a 2M-WS<sub>2</sub> crystal. Starting from low intensity 633 nm, the Raman spectrum shows typical 2M-WS<sub>2</sub> vibrations (black). Then, switching to high intensity 532 nm laser, the Raman spectrum shows typical 2H-WS<sub>2</sub> vibrations (red). Finally, switch laser back to the low intensity 633 nm still produces 2H-WS<sub>2</sub>'s Raman spectrum (blue). (d,e) Differential scanning calorimetry (DSC) of 2M-WS<sub>2</sub> made by conditions i (d) and ii (e). Both samples' heat-flow curvature changes upon heating, but no changes during cooling, suggesting irreversible phase transformation. (f) PXRD of the crystals after DSC measurements. The patterns match with the 2H phase.

We further confirmed materials retain the 2H phase after laser irritation or heating (Figure 5c). For this, we first confirmed a crystal's 2M structure with a low-intensity laser of 633 nm (black) and subsequently irradiated the same spot with 532 nm light, using an intensity that could introduce phase transformation; the resulting Raman spectrum shows transformation to the 2H phase. Finally, we probed the same spot with the low-intensity 633 nm laser, which originally did not induce phase transformation. The Raman spectrum still shows typical 2H vibrations (blue).

Both laser power and intensity must be known to calculate the power intensity threshold that can induce the phase transformation. However, with our Raman setup, the lowest laser intensity we could access still saturates the camera. Therefore, we could not estimate an accurate laser beam size to calculate laser intensities. Since we observed that the phase transformation is independent of the wavelength but sensitive to the power of the laser, it seems likely that the generated heat causes the phase transformation.

To further explore the phase transformation temperature, we performed DSC on the 2M-WS<sub>2</sub> made by both dilute acids (i) and (ii). An exothermic peak, indicative of a phase transformation, appears at 228.0 and 223.7 °C for crystals made with methods (i) and (ii), respectively (Figure 5d,e). Both temperatures are slightly higher than previously reported for the 2M-WS<sub>2</sub> made via  $I_2$  oxidation,<sup>30</sup> as well as for  $H_xWS_2$ . The cooling curve indicates again that phase transformation is irreversible (Figure 5d,e). PXRD on the cooled products confirms these to be the 2H-WS<sub>2</sub> (Figure 5f). A similar phase transformation has also been reported in other TMDs, such as 1T'-MoS<sub>2</sub> and 1T'-MoSe<sub>2</sub>.42 The fact that such a transformation can be induced locally with laser heating suggests that it might be possible to selectively tune the properties of WS<sub>2</sub> flakes as one phase is superconducting/metallic, while the other is semiconducting.

## DISCUSSION

As stated previously, the metastable phase, 2M-WS<sub>2</sub>, is notable for its high superconducting temperature (8.8 K), relative to other TMDs. Thus, it is important to optimize the synthesis method, as well as understand mechanistically the process behind the conversion from K<sub>x</sub>WS<sub>2</sub> to 2M-WS<sub>2</sub>. In this way, we found that the method for making 2M-WS2 influences the superconducting properties. Our results show that using the dilute acid method, without a strong oxidizing agent, increases the superconducting volume fraction. As seen by the increased negative magnetic susceptibility of the nitric acid and sulphuric acid, compared to that prepared by condition (iii), as well as the larger superconducting jumps seen by the former with respect to the latter. This trend was consistent over multiple trials, shown in the Supporting Information, and suggests that the gentler method of using dilute acid yields higher-quality crystals. Such differences were not noticeable in the HRSTEM and SAED images, which may speak to the sensitivity of superconductivity; defects, unseen with PRXD and local probes such as HRSTEM, can still influence the sample's properties.

One point worth noting is why 2M-WS $_2$  shows such a high superconducting temperature, especially compared to other superconducting group 6 TMDs. To understand this, it is worth discussing the metal—metal (M-M) bond distances in those TMDs. In the 1T' structure, which makes up the layers of the 2M phase, M atoms form zigzag chains, resulting in

shorter and longer distances between them. These chains can be viewed as a Peierls-type distortion of the equally spaced atoms that make up the hexagonal lattice of the 1T phase. Since Peierls distortions create a more stabilized system, a higher distortion is indicative of a more stable structure, whereas a smaller distortion would indicate a structural instability. 43 A higher distortion is characterized by a larger difference in M-M distances. A distance ratio of 1 indicates the least stable, undistorted 1T phase, whereas a ratio smaller than 1 indicates the distorted 1T'-phase, and the smaller it gets (within the limits of Coulomb repulsion), the higher the energy gain of the distortion. Since superconductivity often appears close to an electronic instability,  $^{44-46}$  it follows that  $T_c$ could correlate with this ratio. This may explain the lack of superconductivity in (ungated) WTe<sub>2</sub>, where the 1T' phase is the most thermodynamically stable. To this case, the ratio of short and long W–W distance ( $\alpha$ , see derivation in the SI) is 0.818,<sup>47</sup> much smaller than we observe in 2M-WS<sub>2</sub> (0.864). MoTe<sub>2</sub> is most stable in the 2H phase, but the 1T' phase can be synthesized directly if the reaction vessel is quenched from high temperature.<sup>48</sup> 1T'-MoTe<sub>2</sub> is superconducting below 0.1 K, $^{26}$  a much lower  $T_c$  than 2M-WS<sub>2</sub>. Here the Mo–Mo distance ratio is 0.834. $^{48}$  These values suggest a trend: the closer the ratio is to 1 (or the 1T phase), the more robust superconductivity should be.

While much of this paper has focused on our new method for obtaining superconducting 2M-WS $_2$ , our brief mention of 2H-WS $_2$  has practical implications as well. The difficulties of synthesizing 2M-WS $_2$  posed by its metastability provide an opportunity to easily transition to the stable 2H-phase. As a result, there is potential to create a material with a superconducting/semiconducting interface. Our method opens up new research possibilities for creating these materials and studying their properties, as well as potential device applications.

## CONCLUSIONS

In conclusion, our studies have shown that the potassium in K<sub>0.5</sub>WS<sub>2</sub> spontaneously deintercalates from the parent compound when left in humid air or water. With merely a dilute non-oxidative acid, H<sub>2</sub>SO<sub>4</sub> or HNO<sub>3</sub>, it is possible to fully remove K<sup>+</sup> and synthesize the superconducting 2M-WS<sub>2</sub> phase. We have proven with Raman and GC that the Kdeintercalation is not a proton exchange process since S-H was not present in the product, and H2 was produced during the reaction. From this, we can infer that this is an oxidative reaction, where W in K<sub>0.5</sub>WS<sub>2</sub> is oxidized, and H<sup>+</sup> is reduced to H<sub>2</sub> gas. With TGA, Raman spectroscopy, and DFT calculations, we have found that any water molecules in the crystal are associated with the remaining K+. Our PXRD and HRSTEM studies reveal that the 2M-WS<sub>2</sub> made with HNO<sub>3</sub>, H<sub>2</sub>SO<sub>4</sub>, and highly oxidative K<sub>2</sub>Cr<sub>2</sub>O<sub>7</sub> in H<sub>2</sub>SO<sub>4</sub> are indistinguishable from each other by these characterization techniques. However, while d.c. magnetic susceptibility measurements show that the 2M-WS<sub>2</sub> made by all three methods has the same superconducting transition temperature, the magnetic susceptibility was more negative with the less aggressive conditions. Meanwhile, heat capacity measurements reveal that 2M-WS<sub>2</sub>, made with the less aggressive conditions, has a higher superconducting jump. From this, we find that superconductivity is far more sensitive to structural differences than traditional structural characterization techniques. We also showed that the heat generated by a laser, regardless of its

wavelength, can cause the 2M phase to transform into the thermodynamically stable 2H phase. Our study enables future growth of high-quality superconducting 2M-WS<sub>2</sub>, which hopefully will lead to many studies about the potential interplay of topology and superconductivity in crystals with sufficient purity.

## ASSOCIATED CONTENT

## **Supporting Information**

The Supporting Information is available free of charge at https://pubs.acs.org/doi/10.1021/acs.chemmater.3c00813.

Gas chromatography (GC) analysis of the generated gas bubbles; Exploration of reaction time with SEM and EDS; TGA analysis of the interstitial water of K-deintercalation products; Rietveld refinement of PXRD from each method; Calculated Raman spectra; Temperature dependent magnetic susceptibility showing repeatable trends; Calculation of Debye temperature; Mathematical derivation of the relationship of d and  $\alpha$  (PDF)

#### AUTHOR INFORMATION

### **Corresponding Author**

Leslie M. Schoop — Department of Chemistry, Princeton University, New Jersey 08544 Princeton, United States; orcid.org/0000-0003-3459-4241; Email: lschoop@princeton.edu

## Authors

**Xiaoyu Song** — Department of Chemistry, Princeton University, New Jersey 08544 Princeton, United States; ⊚ orcid.org/0000-0003-3384-0527

Brianna Hoff – Department of Chemistry, Princeton University, New Jersey 08544 Princeton, United States Ratnadwip Singha – Department of Chemistry, Princeton University, New Jersey 08544 Princeton, United States;

orcid.org/0000-0002-3155-2137

Joseph W. Stiles – Department of Chemistry, Princeton University, New Jersey 08544 Princeton, United States; orcid.org/0000-0003-3128-036X

Grigorii Skorupskii — Department of Chemistry, Princeton University, New Jersey 08544 Princeton, United States

Jason F. Khoury — Department of Chemistry, Princeton University, New Jersey 08544 Princeton, United States; orcid.org/0000-0003-4769-6730

Guangming Cheng — Princeton Materials Institute, New Jersey 08544 Princeton, United States; orcid.org/0000-0001-5852-1341

Franziska Kamm – Institute of Inorganic Chemistry, University of Regensburg, D-93040 Regensburg, Germany

Ayelet J. Uzan – Department of Physics, Princeton University, New Jersey 08544 Princeton, United States

Stephanie Dulovic — Department of Chemistry, Princeton University, New Jersey 08544 Princeton, United States; orcid.org/0000-0003-0921-9714

Sanfeng Wu − Department of Physics, Princeton University, New Jersey 08544 Princeton, United States; ocid.org/ 0000-0002-6227-6286

Florian Pielnhofer — Institute of Inorganic Chemistry, University of Regensburg, D-93040 Regensburg, Germany Nan Yao — Princeton Materials Institute, New Jersey 08544
Princeton, United States; orcid.org/0000-0002-40811495

Complete contact information is available at: https://pubs.acs.org/10.1021/acs.chemmater.3c00813

#### **Author Contributions**

<sup>1</sup>X.S. and B.H. contributed equally to this work.

#### Notes

The authors declare no competing financial interest.

#### ACKNOWLEDGMENTS

This research was supported by the DOD's Office of Naval Research (ONR) (award number N00014-21-1-2733), the Princeton Center for Complex Materials, a National Science Foundation (NSF)-MRSEC program (DMR-2011750), and the Gordon and Betty Moore Foundation's EPIQS initiative (grant number GBMF9064). The authors acknowledge the use of Princeton's Imaging and Analysis Center, which is partially supported by the Princeton Center for Complex Materials, a National Science Foundation (NSF)-MRSEC program (DMR-2011750). B.L.H. is supported by the NSF Graduate Research Fellowship Program under grant number DGE-2039656. J.F.K. was supported by an Arnold O. Beckman postdoctoral fellowship. S.W. acknowledges the support from AFOSR Young Investigator Program under award number FA9550-23-1-0140. The authors thank Prof. Craig B. Arnold for his insightful discussions about the phase transformation phenomena. The authors thank members of the Schoop lab for their helpful discussions of this manuscript. The authors thank Prof. Jian Sun from Nanjing University for providing us the CIF files of WTe<sub>2</sub> from his DFT calculations of a previous work, 49 and Prof. Jung-Fu Lin and Joon-Seok Kim from the University of Texas at Austin for assisting in obtaining these files.

## **■** REFERENCES

- (1) Gutiérrez, H. R.; Perea-López, N.; Elías, A. L.; Berkdemir, A.; Wang, B.; Lv, R.; López-Urías, F.; Crespi, V. H.; Terrones, H.; Terrones, M. Extraordinary room-temperature photoluminescence in triangular WS<sub>2</sub> monolayers. *Nano Lett.* **2013**, *13*, 3447–3454.
- (2) Cong, C.; Shang, J.; Wang, Y.; Yu, T. Optical properties of 2D semiconductor WS<sub>2</sub>. Adv. Opt. Mater. **2018**, 6, No. 1700767.
- (3) Tongay, S.; Fan, W.; Kang, J.; Park, J.; Koldemir, U.; Suh, J.; Narang, D. S.; Liu, K.; Ji, J.; Li, J.; et al. Tuning interlayer coupling in large-area heterostructures with CVD-grown MoS<sub>2</sub> and WS<sub>2</sub> monolayers. *Nano Lett.* **2014**, *14*, 3185–3190.
- (4) Perea-López, N.; Elías, A. L.; Berkdemir, A.; Castro-Beltran, A.; Gutiérrez, H. R.; Feng, S.; Lv, R.; Hayashi, T.; López-Urías, F.; Ghosh, S.; et al. Photosensor device based on few-layered WS<sub>2</sub> films. *Adv. Funct. Mater.* **2013**, 23, 5511–5517.
- (5) Lin, Y.; Adilbekova, B.; Firdaus, Y.; Yengel, E.; Faber, H.; Sajjad, M.; Zheng, X.; Yarali, E.; Seitkhan, A.; Bakr, O. M.; et al. 17% efficient organic solar cells based on liquid exfoliated WS<sub>2</sub> as a replacement for PEDOT: PSS. *Adv. Mater.* **2019**, *31*, No. e1902965.
- (6) Hong, X.; Kim, J.; Shi, S.-F.; Zhang, Y.; Jin, C.; Sun, Y.; Tongay, S.; Wu, J.; Zhang, Y.; Wang, F. Ultrafast charge transfer in atomically thin MoS<sub>2</sub>/WS<sub>2</sub> heterostructures. *Nat. Nanotechnol.* **2014**, *9*, 682–686
- (7) Lei, T.; Chen, W.; Huang, J.; Yan, C.; Sun, H.; Wang, C.; Zhang, W.; Li, Y.; Xiong, J. Multi-functional layered WS<sub>2</sub> nanosheets for enhancing the performance of lithium—sulfur batteries. *Adv. Energy Mater.* **2017**, *7*, No. 1601843.
- (8) Lin, W.-H.; Wu, P. C.; Akbari, H.; Rossman, G. R.; Yeh, N.-C.; Atwater, H. A. Electrically Tunable and Dramatically Enhanced Valley-Polarized Emission of Monolayer  $WS_2$  at Room Temperature

- with Plasmonic Archimedes Spiral Nanostructures. Adv. Mater. 2022, 34, No. e2104863.
- (9) Jin, C.; Kim, J.; Utama, M. I. B.; Regan, E. C.; Kleemann, H.; Cai, H.; Shen, Y.; Shinner, M. J.; Sengupta, A.; Watanabe, K.; et al. Imaging of pure spin-valley diffusion current in WS<sub>2</sub>-WSe<sub>2</sub> heterostructures. *Science* **2018**, *360*, 893–896.
- (10) Cheng, L.; Huang, W.; Gong, Q.; Liu, C.; Liu, Z.; Li, Y.; Dai, H. Ultrathin WS<sub>2</sub> nanoflakes as a high-performance electrocatalyst for the hydrogen evolution reaction. *Angew. Chem.* **2014**, *126*, 7994–7997.
- (11) Mahler, B.; Hoepfner, V.; Liao, K.; Ozin, G. A. Colloidal synthesis of 1T-WS<sub>2</sub> and 2H-WS<sub>2</sub> nanosheets: applications for photocatalytic hydrogen evolution. *J. Am. Chem. Soc.* **2014**, *136*, 14121–14127.
- (12) Xie, L.; Wang, L.; Zhao, W.; Liu, S.; Huang, W.; Zhao, Q. WS<sub>2</sub> moiré superlattices derived from mechanical flexibility for hydrogen evolution reaction. *Nat. Commun.* **2021**, *12*, 5070.
- (13) Wypych, F.; Sollmann, K.; Schöllhorn, R. Metastable layered chalcogenides 1T-MoS<sub>2</sub>, 2M-WS<sub>2</sub> and 1T-Mo<sub>12</sub>W<sub>12</sub>S<sub>2</sub>: electrochemical study on their intercalation reactions. *Mater. Res. Bull.* **1992**, 27, 545–553.
- (14) Manzeli, S.; Ovchinnikov, D.; Pasquier, D.; Yazyev, O. V.; Kis, A. 2D transition metal dichalcogenides. *Nat. Rev. Mater.* **2017**, 2, 17033
- (15) Qian, X.; Liu, J.; Fu, L.; Li, J. Quantum spin Hall effect in two-dimensional transition metal dichalcogenides. *Science* **2014**, *346*, 1344–1347.
- (16) Fang, Y.; Pan, J.; Zhang, D.; Wang, D.; Hirose, H. T.; Terashima, T.; Uji, S.; Yuan, Y.; Li, W.; Tian, Z.; et al. Discovery of superconductivity in 2M WS<sub>2</sub> with possible topological surface states. *Adv. Mater.* **2019**, *31*, No. 1901942.
- (17) Yuan, Y.; Pan, J.; Wang, X.; Fang, Y.; Song, C.; Wang, L.; He, K.; Ma, X.; Zhang, H.; Huang, F.; et al. Evidence of anisotropic Majorana bound states in 2M-WS<sub>2</sub>. *Nat. Phys.* **2019**, *15*, 1046–1051.
- (18) Li, Y.; Zheng, H.; Fang, Y.; Zhang, D.; Chen, Y.; Chen, C.; Liang, A.; Shi, W.; Pei, D.; Xu, L.; et al. Observation of topological superconductivity in a stoichiometric transition metal dichalcogenide 2M-WS<sub>2</sub>. *Nat. Commun.* **2021**, *12*, 2874.
- (19) Wang, L.; Fang, Y.; Huang, Y.; Cheng, E.; Ni, J.; Pan, B.; Xu, Y.; Huang, F.; Li, S. Nodeless superconducting gap in the topological superconductor candidate 2M-WS<sub>2</sub>. *Phys. Rev. B* **2020**, *102*, No. 024523.
- (20) Lian, C.-S.; Si, C.; Duan, W. Anisotropic full-Gap superconductivity in 2M-WS<sub>2</sub> topological metal with intrinsic proximity effect. *Nano Lett.* **2021**, *21*, 709–715.
- (21) Sajadi, E.; Palomaki, T.; Fei, Z.; Zhao, W.; Bement, P.; Olsen, C.; Luescher, S.; Xu, X.; Folk, J. A.; Cobden, D. H. Gate-induced superconductivity in a monolayer topological insulator. *Science* **2018**, 362, 922–925.
- (22) Fatemi, V.; Wu, S.; Cao, Y.; Bretheau, L.; Gibson, Q. D.; Watanabe, K.; Taniguchi, T.; Cava, R. J.; Jarillo-Herrero, P. Electrically tunable low-density superconductivity in a monolayer topological insulator. *Science* **2018**, *362*, 926–929.
- (23) Kang, D.; Zhou, Y.; Yi, W.; Yang, C.; Guo, J.; Shi, Y.; Zhang, S.; Wang, Z.; Zhang, C.; Jiang, S.; et al. Superconductivity emerging from a suppressed large magnetoresistant state in tungsten ditelluride. *Nat. Commun.* **2015**, *6*, 7804.
- (24) Pan, X.-C.; Chen, X.; Liu, H.; Feng, Y.; Wei, Z.; Zhou, Y.; Chi, Z.; Pi, L.; Yen, F.; Song, F.; et al. Pressure-driven dome-shaped superconductivity and electronic structural evolution in tungsten ditelluride. *Nat. Commun.* **2015**, *6*, 7805.
- (25) Asaba, T.; Wang, Y.; Li, G.; Xiang, Z.; Tinsman, C.; Chen, L.; Zhou, S.; Zhao, S.; Laleyan, D.; Li, Y.; et al. Magnetic field enhanced superconductivity in epitaxial thin film WTe<sub>2</sub>. Sci. Rep. **2018**, *8*, 6520.
- (26) Qi, Y.; Naumov, P. G.; Ali, M. N.; Rajamathi, C. R.; Schnelle, W.; Barkalov, O.; Hanfland, M.; Wu, S.-C.; Shekhar, C.; Sun, Y.; et al. Superconductivity in Weyl semimetal candidate MoTe<sub>2</sub>. *Nat. Commun.* **2016**, *7*, 11038.

- (27) Guo, C.; Pan, J.; Li, H.; Lin, T.; Liu, P.; Song, C.; Wang, D.; Mu, G.; Lai, X.; Zhang, H.; et al. Observation of superconductivity in 1T'-MoS<sub>2</sub> nanosheets. *J. Mater. Chem. C* **2017**, *5*, 10855–10860.
- (28) Peng, J.; Liu, Y.; Luo, X.; Wu, J.; Lin, Y.; Guo, Y.; Zhao, J.; Wu, X.; Wu, C.; Xie, Y. High Phase Purity of Large-Sized 1T'-MoS<sub>2</sub> Monolayers with 2D Superconductivity. *Adv. Mater.* **2019**, *31*, No. 1900568.
- (29) Song, X.; Singha, R.; Cheng, G.; Yeh, Y.-W.; Kamm, F.; Khoury, J. F.; Hoff, B. L.; Stiles, J. W.; Pielnhofer, F.; Batson, P. E.; et al. Synthesis of an aqueous, air-stable, superconducting 1T'-WS2 monolayer ink. *Sci. Adv.* 2023, *9*, No. eadd6167.
- (30) Lai, Z.; He, Q.; Tran, T. H.; Repaka, D. M.; Zhou, D.-D.; Sun, Y.; Xi, S.; Li, Y.; Chaturvedi, A.; Tan, C.; et al. Metastable 1T'-phase group VIB transition metal dichalcogenide crystals. *Nat. Mater.* **2021**, 20, 1113–1120.
- (31) Song, X.; Cheng, G.; Weber, D.; Pielnhofer, F.; Lei, S.; Klemenz, S.; Yeh, Y.-W.; Filsinger, K. A.; Arnold, C. B.; Yao, N.; et al. Soft Chemical Synthesis of  $H_x$ CrS<sub>2</sub>: An Antiferromagnetic Material with Alternating Amorphous and Crystalline Layers. *J. Am. Chem. Soc.* **2019**, *141*, 15634–15640.
- (32) Song, X.; Schneider, S. N.; Cheng, G.; Khoury, J. F.; Jovanovic, M.; Yao, N.; Schoop, L. M. Kinetics and Evolution of Magnetism in Soft-Chemical Synthesis of CrSe<sub>2</sub> from KCrSe<sub>2</sub>. *Chem. Mater.* **2021**, 33, 8070–8078.
- (33) Yuan, F.; Song, X.; Cheng, G.; Yao, N.; Mozharivskyj, Y.; Schoop, L. M. Magnetic Nanosheets via Chemical Exfoliation of  $K_{2x}Mn_xSn_{1-x}S_2$ . Chem. Mater. **2022**, *34*, 5084.
- (34) Heising, J.; Kanatzidis, M. G. Exfoliated and restacked MoS<sub>2</sub> and WS<sub>2</sub>: Ionic or neutral species? Encapsulation and ordering of hard electropositive cations. *J. Am. Chem. Soc.* **1999**, *121*, 11720–11732.
- (35) Bryant, M. A.; Pemberton, J. E. Surface Raman scattering of self-assembled monolayers formed from 1-alkanethiols: behavior of films at gold and comparison to films at silver. *J. Am. Chem. Soc.* **1991**, 113, 8284–8293.
- (36) Bratsch, S. G. Standard electrode potentials and temperature coefficients in water at 298.15 K. J. Phys. Chem. Ref. Data 1989, 18, 1–21
- (37) Bentley, C. L.; Bond, A. M.; Hollenkamp, A. F.; Mahon, P. J.; Zhang, J. Voltammetric determination of the iodide/iodine formal potential and triiodide stability constant in conventional and ionic liquid media. *J. Phys. Chem. C* **2015**, *119*, 22392–22403.
- (38) Li, S.; Zeng, B.; Wan, X.; Tao, J.; Han, F.; Yang, H.; Wang, Z.; Wen, H.-H. Anomalous properties in the normal and superconducting states of LaRu<sub>3</sub>Si<sub>2</sub>. *Phys. Rev. B* **2011**, *84*, No. 214527.
- (39) Gui, X.; Cava, R. J. LaIr3Ga2: a superconductor based on a kagome lattice of Ir. Chem. Mater. 2022, 34, 2824-2832.
- (40) McMillan, W. Transition temperature of strong-coupled superconductors. *Phys. Rev.* **1968**, *167*, 331.
- (41) Pierucci, D.; Zribi, J.; Livache, C.; Gréboval, C.; Silly, M. G.; Chaste, J.; Patriarche, G.; Montarnal, D.; Lhuillier, E.; Ouerghi, A.; et al. Evidence for a narrow band gap phase in 1T' WS<sub>2</sub> nanosheet. *Appl. Phys. Lett.* **2019**, *115*, No. 032102.
- (42) Yu, Y.; Nam, G.-H.; He, Q.; Wu, X.-J.; Zhang, K.; Yang, Z.; Chen, J.; Ma, Q.; Zhao, M.; Liu, Z.; et al. High phase-purity 1T'-MoS<sub>2</sub>-and 1T'-MoSe<sub>2</sub>-layered crystals. *Nat. Chem.* **2018**, *10*, 638–643.
- (43) Hoffmann, R. How chemistry and physics meet in the solid state. *Angew. Chem. Int. Ed. Engl.* 1987, 26, 846–878.
- (44) Luo, H.; Xie, W.; Tao, J.; Pletikosic, I.; Valla, T.; Sahasrabudhe, G. S.; Osterhoudt, G.; Sutton, E.; Burch, K. S.; Seibel, E. M.; et al. Differences in Chemical Doping Matter: Superconductivity in Ti<sub>1-x</sub>Ta<sub>x</sub>Se<sub>2</sub> but Not in Ti<sub>1-x</sub>Nb<sub>x</sub>Se<sub>2</sub>. *Chem. Mater.* **2016**, *28*, 1927–1935
- (45) Wagner, K.; Morosan, E.; Hor, Y.; Tao, J.; Zhu, Y.; Sanders, T.; McQueen, T.; Zandbergen, H.; Williams, A.; West, D.; et al. Tuning the charge density wave and superconductivity in Cu<sub>x</sub>TaS<sub>2</sub>. *Phys. Rev. B* **2008**, *78*, No. 104520.

**Chemistry of Materials** Article pubs.acs.org/cm

- (46) Schoop, L. M.; Müchler, L.; Felser, C.; Cava, R. Lone pair effect, structural distortions, and potential for superconductivity in Tl perovskites. Inorg. Chem. 2013, 52, 5479-5483.
- (47) Brixner, L. H. Preparation and properties of the single crystalline AB2-type selenides and tellurides of niobium, tantalum, molybdenum and tungsten. *J. Inorg. Nucl. Chem.* **1962**, 24, 257–263. (48) Brown, B. E. The crystal structures of WTe<sub>2</sub> and high-
- temperature MoTe<sub>2</sub>. Acta Crystallogr. 1966, 20, 268-274.
- (49) Lu, P.; Kim, J.-S.; Yang, J.; Gao, H.; Wu, J.; Shao, D.; Li, B.; Zhou, D.; Sun, J.; Akinwande, D.; et al. Origin of superconductivity in the Weyl semimetal WTe2 under pressure. Phys. Rev. B 2016, 94, No. 224512.